Structure Model of a Poly(vinyl alcohol) Film Uniaxially Stretched in Water and the Role of Crystallites on the Stress−Strain Relationship

Tsukasa Miyazaki,*,† Akie Hoshiko,† Midori Akasaka,† Miki Sakai,† Yuuki Takeda,† and Shinichi Sakurai‡

Core Technology Center, Nitto Denko Corporation, 1-1-2, Shimohozumi, Ibaraki, Osaka 567-8680, Japan, and Department of Polymer Science & Engineering, Kyoto Institute of Technology, Matsugasaki, Sakyo-ku, Kyoto 606-8585, Japan

Received March 27, 2007; Revised Manuscript Received August 31, 2007

ABSTRACT: We propose a structure model of a poly(vinyl alcohol) (PVA) film during uniaxial stretching in water. In addition to the relaxation of microfibrils and the extension of interfibrillar amorphous regions shown in our previous paper, it was described that the strain-induced crystallization takes place in the interfibrillar extended amorphous regions, which bear the increasing stress with strain, by conducting simultaneously the tensile stress−strain measurement with the wide-angle X-ray diffraction (WAXD) measurements for the film stretched in water. Furthermore, we examined the dissolution behavior of the PVA film in water by using in-situ WAXD and small-angle X-ray scattering. It was concluded that the dissolution of crystallites in the lamellar stacks, which are considered to be precursors of the microfibrils formed with film stretching, softens the system, as shown with the stress−strain measurement in water above 333 K, leading to the ineffective amorphous chain extension of PVA molecules.

1. Introduction

Poly(vinyl alcohol) (PVA) has been widely used in various industrial applications, such as high-quality polarizers, high-strength fibers, and so on.[1] In the past decade, PVA has been promising as a substrate of polarizers used in liquid crystalline displays, which have been widely applied to televisions and monitors of cellular phones. PVA films are very suitable to the application to polarizers because they possess high ability of PVA−iodine complex formation in the film microstructure.[1]

When PVA films are soaked in a KI/I_2 aqueous solution, adsorbed iodines are one-dimensionally aligned along with the orientation of PVA chains by the film drawing, followed by the formation of PVA−iodine complexes, which show extremely high ability of dichromatic performance. The structure model of the PVA−iodine complex proposed by Miyasaka et al.[2,3] and Takamiya et al.,[4] who suggested that polyiodine ions are surrounded with the aggregates of extended sequences in the PVA molecular chains, seems to be reasonable compared to other models previously proposed, such as the helix model.[5,6] However, the mechanism for the formation and orientation of the iodine complexes has not been revealed in spite of various efforts.

It was suggested that PVA−iodine complexes are formed in amorphous regions in PVA films, when the films are soaked in a KI/I_2 aqueous solution with a relatively low iodine concentration,[2] such as that used in the preparation of polarizers. Therefore, it is very important to investigate the orientation of the molecular chains in the film microstructure, especially in the amorphous regions, because the high dichromatic performance of the polarizers should be attributed to the PVA−iodine complexes with a high degree of orientation in amorphous regions.

* To whom correspondence should be addressed: e-mail tsukasa_miyazaki@gg.nitto.co.jp; Ph +81-72-621-0265; Fax +81-72-621-0316.

† Nitto Denko Corporation.

‡ Kyoto Institute of Technology.

For elucidating the development of the orientation of PVA molecular chains in amorphous regions with strain, we have investigated the structure changes in a PVA film during uniaxial deformation in water without molecular chain relaxation by using simultaneous measurements of small-angle X-ray scattering (SAXS) and the tensile stress−strain relationship.[7] Consequently, we could construct the structure model describing the continuous structure changes of the PVA film during uniaxial deformation in water. This structure model includes the elastic expansion of the interlamellar amorphous regions, lamellar breakup, fibrillation, and extension of interfibrillar amorphous regions according to the film stretching.

In this article, we present a further detailed structure model of the PVA film uniaxially stretched in water. This final version of the structure model contains the strain-induced crystallization in the interfibrillar amorphous regions confirmed with the simultaneous stress−strain and wide-angle X-ray diffraction (WAXD) measurements during uniaxial deformation. Furthermore, we have investigated the dissolving behaviors of the PVA film in water for elucidating the role of crystallites on the stress−strain behaviors. It is expected that this structural study on the microstructure of the PVA film must lead to the development of a polarizer with high dichromatic performance.

2. Experimental Section

2.1. PVA Films. The PVA films made by Kuraray Co. (Vinylon) with the degree of polymerization of 2400 were used in this study. The triad tacticity ($mm = 0.21$, $mr = 0.50$, $rr = 0.29$) was determined in solution state by ^{1}H NMR spectroscopy. The films also had a high degree of saponification, which is larger than 99 mol %. The thickness of the PVA films was 0.075 mm. The films were rinsed in ionized water for further purification.

2.2. Tensile Testing. The stress−strain curves for the films in water were obtained by a tensile testing apparatus (AUTO GRAPH AG-100E; Shimadzu Corp.) with a special designed homemade water bath for the investigation of the films in water. Water temperature was regulated with a temperature controller in the range of 278−353 K. Rectangular-shaped specimens of gauge dimensions 30×20 mm^2 in the dried state were examined.

10.1021/ma070731k CCC: $37.00
Published on Web 10/18/2007

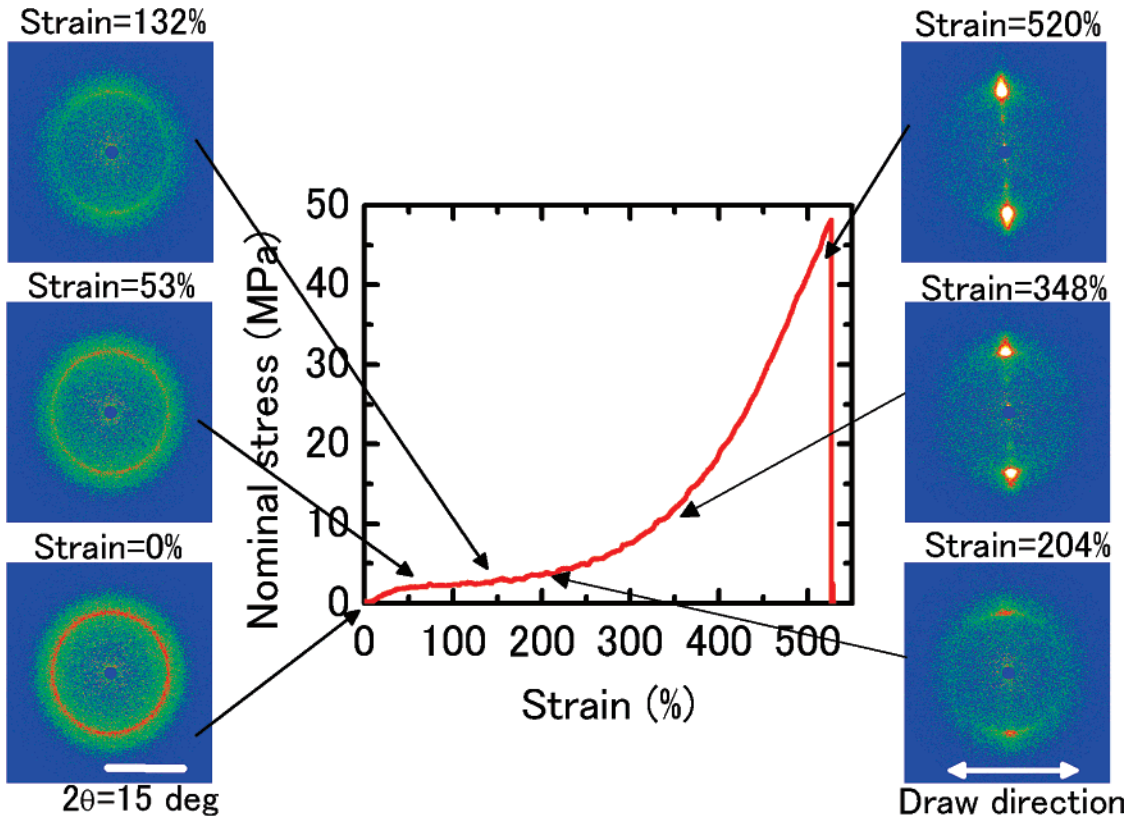

Figure 1. Stress−strain curve and typical 2-D WAXD patterns collected during uniaxial deformation in water at 298 K. Each pattern was obtained in 15 s from the point indicated by each arrow.

2.3. Simultaneous Stress−Strain/WAXD Measurements. Simultaneous stress−strain/WAXD experiments were performed with the WAXD apparatus at BL40B2 beamline of SPring-8 (Japan Synchrotron Radiation Research Institute, Hyogo, Japan). The wavelength of X-rays was turned at 0.1 nm for the WAXD experiments at BL40B2. The beam size was 0.8 mm × 0.5 mm, allowing the examination over a relatively large area rather than a local area of the film. The camera length of the WAXD apparatus was 190.4 mm. The CCD detector system bearing an image intensifier was used to allow a rapid scan of two-dimensional (2-D) WAXD patterns from the samples during uniaxial stretching in water. The calibration of the scattering angle was carried out using diffraction from a regular structure in a polyethylene film and the Si powder purchased from the National Institute of Standards and Technology.

Our newly developed stretch machine was used in the simultaneous WAXD and stress−strain experiments at BL40B2 beamline. The stretch machine was described in our previous paper in detail.[7] Therefore, only an outline about this stretch machine is described here. This stretch machine allows a film sample to be stretched symmetrically in the lateral direction, which assures that X-ray beam always illuminates the same position of the sample during film stretching. Moreover, this instrument equips a water bath which can be jacked up and down so as to enclose and disclose the film specimen. The water bath has holes for the beam path, which are covered with two polyimide windows with a thickness of 25 μm. The gap between the two polyimide windows is 1 mm, in which water and the film are placed. The temperature of water can be controlled in a range from room temperature to 373 K using a temperature controller with an accuracy of ±1 K. The length and the width of the film are 30 and 20 mm, respectively.

The selected stretching speed was 5 mm/min (17% strain/min). Each 2-D WAXD pattern was accumulated in 15 s every an acquisition period of 30 s using the CCD detector along with a drawing. Therefore, a 2-D WAXD pattern was attributed to an averaged structure during deformation in 15 s. The 2-D WAXD pattern measured for water was subtracted as a background noise without transmittance correction because the transmittance of the samples in water was identical to that of water background.

For four films we repeated the simultaneous experiments under the same experimental conditions, so as to confirm that the structural variations observed at the X-ray beam position are representative of the observed bulk mechanical properties in the stress−strain curve simultaneously measured. In these four experiments, the similar structural parameters were obtained with the data analysis of the 2-D WAXD patterns as described in the next section during uniaxial deformation, indicating that the structural parameters obtained at the X-ray beam position are representative of the observed bulk stress−strain relationship.

3. Results

3.1. Simultaneous Stress−Strain/WAXD Measurements. A stress−strain curve and typical 2-D scattering patterns obtained simultaneously during uniaxial deformation in water at 298 K are shown in Figure 1. Each arrow drawn from the 2-D patterns to the stress−strain curve in the figure indicates the strain at which the 2-D pattern was obtained.

The stress−strain relationship completely follows the stress−strain behavior indicated in our previous paper, similar to the one of a cross-linked rubber with an ability of strain-induced crystallization. The strain-induced hardening occurs at the strain of about 200%, as shown in our previous paper.[7]

In the 2-D scattering pattern of the undeformed film, a circular scattering pattern with a homogeneous intensity distribution along the circle is observed at the scattering angle, 2θ, of about 12.3°, which can be identical to the Debye ring from the (101)-($10\bar{1}$) doublet of the PVA crystallites.[1,2] This circular diffraction concentrates on the transversal direction with strain, resulting in a high degree of orientation of crystallites above the strain of 200%, as shown in Figure 1. This transversal sharp diffraction may be originated from the oriented amorphous phase or so-called mesophase. However, the radial peak position of the diffraction remains nearly constant with strain, and the degree of orientation derived from the azimuthal intensity profile is

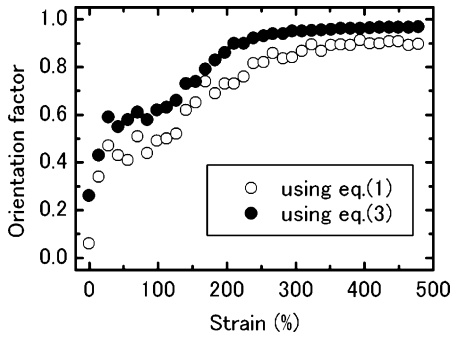

Figure 2. Orientation distribution function of the molecular chains during uniaxial deformation in water. The open and closed circles were obtained by using eqs 1 and 3 in the text, respectively.

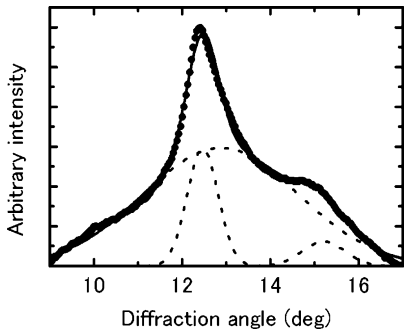

Figure 3. Typical example of the peak decomposition of an azimuthally integrated intensity profile for a 2-D WAXD pattern of an undrawn PVA film in water. Points are experimental data. Lines are the best fitting curves.

relatively high (see Figure 2) compared to that of the molecular chains observed generally in amorphous or mesophase components. Furthermore, in infrared absorption spectra for PVA films, the crystalline absorption band of 1142 cm^{-1} was assigned by Tadokoro et al.[8] We have investigated the orientation of this band by polarized infrared absorption spectroscopy for a wetted thin PVA film in the fixed end, which was pulled up in air after stretching in water. Unpublished work in our laboratory has shown a high degree of orientation of this crystalline band in this film. Therefore, it was confirmed that the crystallites in the film stretched in water orient to the stretching direction, indicating that this transversal shape diffraction in the 2-D WAXD patterns with a large strain is attributed to the orientation of crystallites.

The degree of orientation of the crystallites increases with strain, attributed to the lamellar orientation, as indicated with the simultaneous stress−strain/SAXS measurements in our previous work.[7] We evaluated the degree of molecular orientation by two methods. One of these two methods is the examination of the second-order moment of the orientation distribution function of the molecular chains. We calculated the second-order moment of the orientation distribution function by using the 1-D peak intensity distribution of this crystalline diffraction along the azimuthal angle, ϕ, as follows:

$$\langle P_2(\cos\phi)\rangle = \frac{2}{3\cos^2\sigma - 1}\frac{3\langle\cos^2\phi\rangle - 1}{2} \qquad (1)$$

where σ is the angle between the normal to the $(101)(10\bar{1})$ planes and the molecular chain axis. The average $\langle\cos^2\phi\rangle$ is calculated by integrating the intensity of specific 2θ diffraction peak along the ϕ, as follows:

$$\langle\cos^2\phi\rangle = \frac{\int_0^{\pi/2} I(\phi)\cos^2\phi\sin\phi\,d\phi}{\int_0^{\pi/2} I(\phi)\sin\phi} \qquad (2)$$

Here, $I(\phi)$ is the 1-D intensity distribution along with the azimuthal angle after the subtraction of the background intensity.

The second method for estimating the orientation of the molecular chains is the examination of the full width at half-maximum (fwhm) of the azimuthal profile fitted with an appropriate fitting function. We fit the azimuthal scattering profile at the radial scattering maximum of the crystalline peak intensity with Pearson VII function by using the multiple peak fitting module of Origin Pro version 7.5, which is also used for the various peak decompositions of the 1-D scattering profiles derived from 2-D WAXD patterns, as described below. Orientation factors are obtained with the fwhms of the fitted Pearson VII function by using the following equation:

$$F = \frac{180 - \text{fwhm}}{180} \qquad (3)$$

Figure 2 shows the orientation factors evaluated with the two methods during film stretching. A common trend of the development of the molecular chain orientation obtained with two methods is also shown in Figure 2. A substantial increase in the degree of molecular chain orientation is observed at the initial stage of deformation below about 50% strain, indicating that the orientation of the crystallites is attributed to the lamellar orientation associated with film stretching shown in the previous stress−strain/SAXS measurements. Above the strain of about 50%, the increase in the orientation factor levels off. The following another substantial increase in the orientation factor is also observed at the strain of 150−200%.

On the other hand, the crystalline peak intensity seems to decrease with strain below the strain of 200%, typically shown in the three patterns at the strains of 53%, 132%, and 204% in Figure 1. For the conventional determination of the apparent crystallinity index of the film during uniaxial deformation, simply, we examined azimuthally integrated 1-D scattering profiles as a function of the strain without further data corrections such as the weighting of sin ϕ for uniaxially oriented systems, where ϕ is the azimuthal angle from the stretch direction, because we must continuously investigate the structure changes of the film at low strains including the isotropic one and at relatively large strains during uniaxial deformation without systematic errors. These simple azimuthally integrated 1-D profiles were examined in many cases for determining the crystallinity index in films.[9−11] The typical example for the 1-D scattering profile of the undeformed film is shown in Figure 3. For determining of the apparent crystallinity index, the peak decomposition procedure was performed on these 1-D profiles obtained during uniaxial deformation in water. A 1-D scattering profile is decomposed into two crystalline peaks ($(101)(10\bar{1})$ and (200) planes) and one amorphous halo in the examined region. The peak type was chosen to be Gaussian.

The typical fitting result is also including in Figure 3. In the peak fitting procedure, the position and fwhm of the amorphous peak must be floated because these parameters are required to describe the development of the oriented amorphous components with strain. Other parameters (positions, heights, and fwhms of the two crystalline peaks and height of the amorphous peak) are also floated in the fitting routine. The apparent crystallinity index, f_c, is thus determined as follows:

$$f_c = \frac{\sum A_c}{\sum A_c + A_a} \tag{4}$$

where A_c is the integrated area underneath the crystalline peaks and A_a is the integrated area of the amorphous peak.

By using X-ray scattering method, the accurate crystallinity index of dried PVA films can be estimated with such the method proposed by Sakurada.[12] We could not apply this method to our case for the data in the limited range. However, for dried films we indicated that the crystallinity index in the film could be qualitatively estimated using the data in the limited range, such as that shown in Figure 1.[13] This is probably due to week crystalline diffraction intensities out of range in 2-D WAXD patterns obtained for the PVA films used in these studies.

Furthermore, the total scattering profile from the system, $I_{tot}(2\theta)$, is described with the following equation

$$I_{tot}(2\theta) = I_{PVA}(2\theta) + I_{water}(2\theta) + I_{int}(2\theta) \tag{5}$$

where $I_{PVA}(2\theta)$, $I_{water}(2\theta)$, and $I_{int}(2\theta)$ are the scattering profile of the PVA molecules, that of water molecules, and the interference term due to the PVA molecules and adsorbed water molecules in the system, respectively. For the determination of the apparent crystallinity index by X-ray diffraction, the scattering profile from only the PVA molecules in the system, $I_{PVA}(2\theta)$, must be extracted from the observed total scattering profile, $I_{tot}(2\theta)$. Strictly speaking, we must consider the interference term, $I_{int}(2\theta)$, because $I_{int}(2\theta)$ cannot be subtracted by the merely subtraction of the scattering profile of water background ($I_{water}(2\theta)$) from that of the PVA film and water ($I_{tot}(2\theta)$), as described in the Experimental Section. We assume the interference term to be negligible. For the film undrawn in pure water, the crystallinity index determined by using this convenient X-ray method described above was 22−26%, whereas the one determined by a similar X-ray method for the dried film is 34%,[13] which may be an appropriate value or a larger one compared with the case of the film in water. This indicates that this convenient data correction is applicable to the investigation of the apparent crystallinity in the samples in water. The difference between the crystallinity of the PVA film swollen with water and that of the dried one examined by a similar X-ray method may be also due to the dissolution of unperfect or smaller crystallites in water, as described in the next section. However, it should be noticed that this f_c can only be used to compare samples within this experiment only for qualitative trends and that the value of f_c differs from the absolute crystallinity of the PVA samples in water.

In general, X-ray experiments on hydrated specimens are often complicated by severe secondary radiation damage. In our previous study, we investigated the sample degradation of the film in water for 30 min every acquisition period of 30 s (accumulation time of 1.5 s) by examining the scattering invariant in SAXS patterns at BL45XU (light source; undulator) of SPring-8. For 30 min, the scattering invariant remains constant, indicating that the X-ray radiation does not affect the lamellar structure in the film in water. Therefore, in this study, we can infer that the X-ray radiation in the simultaneous measurements does not affect the structure parameters in the film, such as the crystallinity index, because the flux of the incident X-rays at BL40B2 (light source; bending magnet) used in this study is reduced to about 2 orders lower compared to the one at BL45XU.

Figure 4 shows the crystallinity index of the film with strain. Below the strain of about 200%, the crystallinity decreases with strain, whereas it begins to increase with strain above the 200% strain, indicating that the strain-induced crystallization occurs above the strain of about 200%. The inset in Figure 4 indicates the peak height around the main crystalline peak with strain. The peak height increases above the strain of 200% with strain despite the decrease in the scattering volume associated with film stretching, also clearly indicating the occurrence of the strain-induced crystallization. Therefore, we conclude that the strain-induced crystallization occurs above the strain of about 200%. Watase et al. reported that the strain-induced crystallization takes place for a PVA gel swollen with water.[14] The strain of about 200% is consistent with the one above which the strain-induced hardening takes place, as shown in this study and the previous one, indicating that the strain-induced hardening in the stress−strain curve must be associated with the strain-induced crystallization.

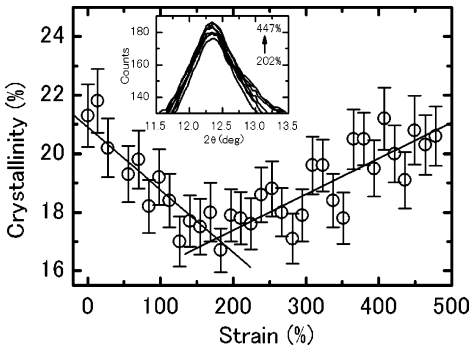

Figure 4. Apparent crystallinity, f_c, for the PVA film during uniaxial deformation in water at 298 K. These crystallinity indexes were determined with the azimuthally integrated 1-D scattering profiles for the 2-D WAXD patterns of the film shown in Figure 1. The inset indicates the peak height around the main crystalline peak with strain.

Below the strain of about 200%, the decrease in the crystallinity may be ascribed to the unfolding of the crystalline chains with the lamellar breakup prior to the fibrillation, which was suggested with the long period decrease above 70% strain, that is to say, the relaxation of the interlamellar amorphous regions with strain, as described in our previous work.[7]

The transversal crystallite size, l_c, can be evaluated with the crystalline peak width of (101)(10$\bar{1}$) doublet in the transversal 1-D scattering profile by using the following Scherrer equation:

$$l_c = \frac{0.9\lambda}{(\Delta 2\theta)\cos\theta_m} \tag{6}$$

where $\Delta 2\theta$ is the fwhm of the crystalline peak in radian and θ_m is half of the peak angle. For this estimation, the transversal 1-D slice in the direction perpendicular to the stretching direction of the 2-D WAXD patterns are plotted and decomposed into two crystalline peaks and one amorphous peak, such as that carried out for the determination of the f_c with eq 4. The evaluated crystallite sizes with strain are shown in Figure 5. Below the strain of about 200%, the substantial decrease in the transversal crystallite size with strain also indicates the lamellar breakup and the consequent fibrillation. On the other hand, the constancy of the crystallite size of about 5.5 nm from the strain of 200% to a break may be ascribed to the contribution of the new crystallites produced with the strain-induced crystallization as well as the completion of fibrillation. This also indicates that the average fibrillar width is about 5.5 nm, whereas the interfibrillar distance is about 7 nm, which was calculated with the peak position in the transversal streak scattering in our previous SAXS study.[7]

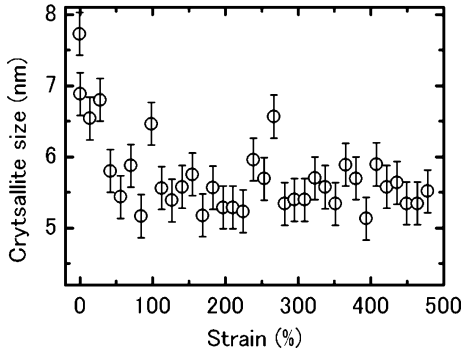

Figure 5. Transversal crystallite size, l_c, for the PVA film during uniaxial deformation in water at 298 K by using the diffraction of the (101)(10$\bar{1}$) doublet oriented to the direction perpendicular to the draw direction.

The relaxation of the interlamellar amorphous regions associated with the lamellar breakup is also confirmed with the development of the molecular orientation shown in Figure 2. Below about 50% strain, the crystalline orientation factor substantially increases with the lamellar orientation in the direction perpendicular to the stretching direction, as mentioned above. However, above the strain of 50% the orientation factor of the crystallites levels off with strain, suggesting the relaxation of the interlamellar amorphous chains associated with the lamellar breakup (Figure 2). The subsequent substantial increase in the crystalline orientation must be due to a high degree of orientation inherent to the strain-induced crystallites formed above the strain of about 200%.

In our previous paper, we studied the degree of swelling of the same film used in this study during uniaxial deformation in water with the examination of the cross section of the film on the film stretching (see Figure 12a,b in ref 7). We found that the degree of swelling of the film increases with strain up to the strain of about 200% and then decreases with film stretching. We attempted to explain this behavior with the strain-induced swelling of gels investigated by Takigawa et al.[15−18] However, this swelling behavior may be simply explained with the crystallinity decrease below 200% strain and the strain-induced crystallization above the strain of 200% described in this study. In our previous work[7] for the swelling behavior of the PVA film by SAXS, it was also confirmed that only amorphous regions are fully swollen with water, whereas the crystalline domains do not absorb water. Therefore, the increase in the degree of film swelling with water up to 200% strain should be attributed to the increase in the amorphous fraction associated with the decrease in crystallinity with strain, whereas the contraction of the film above 200% strain must be attributed to the increase in the volume fraction of crystallites, which is due to the strain-induced crystallization above 200% strain, as shown in Figure 4.

3.2. Dissolution Behavior of the PVA Crystallites in Water. For the undeformed film, the 2-D WAXD patterns were obtained at various temperatures in water, as shown in Figure 6. The crystalline peak originated from (101)(10$\bar{1}$) crystalline planes diminishes with temperature. The azimuthally integrated 1-D scattering profile and the apparent crystallinity index such as those described in the previous section are shown in Figure 7 and the inset of this figure. The crystalline peak intensity and the consequent crystallinity decrease gradually with temperature. At the temperature of 339 K, the crystallinity index is reduced to nearly 0. It is well-known that crystallites in PVA films swollen with water and PVA gels dissolve at a relatively low temperature.[14,19−23] In fact, in the case of PVA gels swollen with water, the dissolution behaviors of PVA crystallites in the gel structure have been investigated by using various experimental techniques such as DSC, X-ray diffraction, and solid-state NMR, indicating that a large amount of crystallites dissolve below 373 K.[14,19−22]

The inset of Figure 7 shows the broad distribution of the size and/or perfection of the crystallites, since there is not a distinct dissolution point, consistent with the PVA gels dissolution

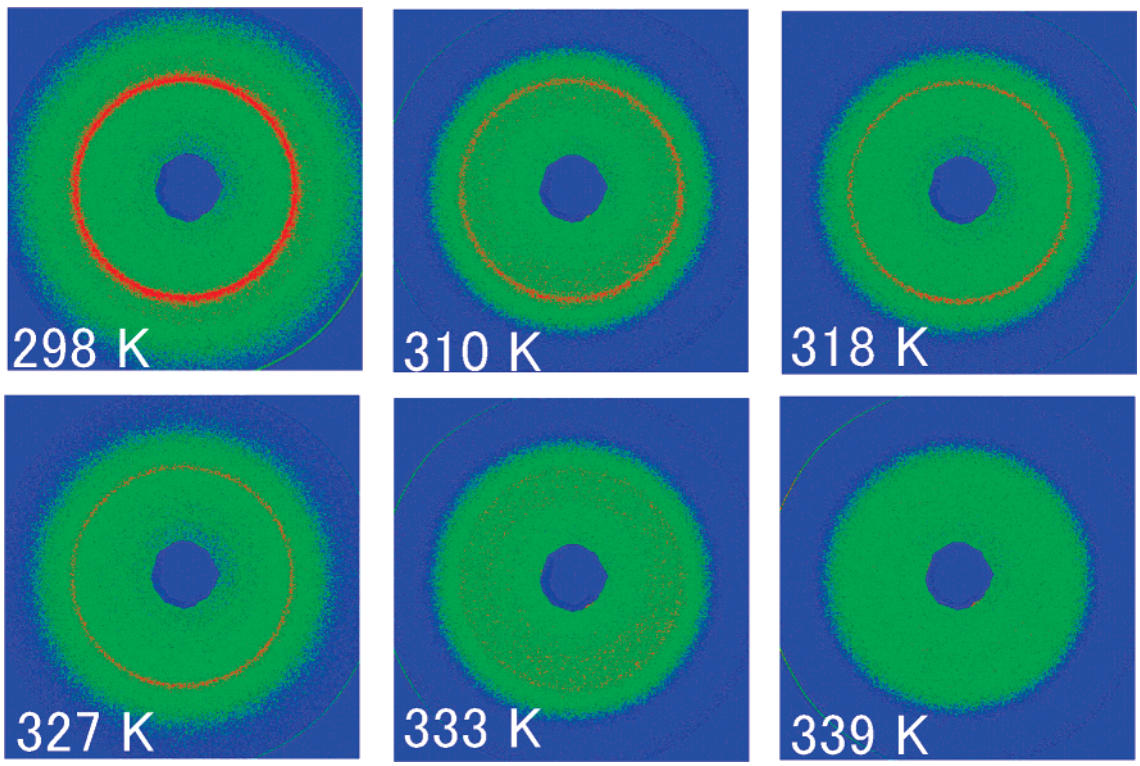

Figure 6. 2-D WAXD patterns for the PVA film undeformed in water at various temperatures indicated in the figure.

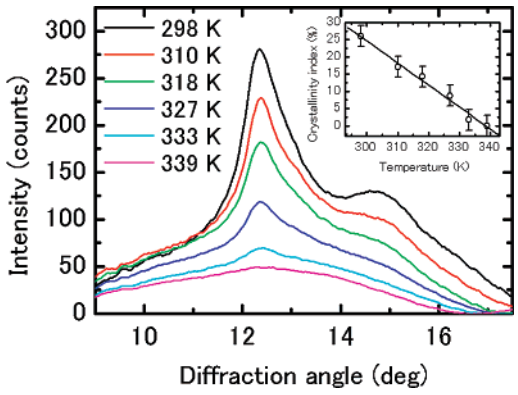

Figure 7. Azimuthally integrated 1-D scattering profiles for the 2-D WAXD patterns shown in Figure 6. Each 1-D profile is vertically shifted for clarity. The inset indicates the apparent crystallinity for these profiles.

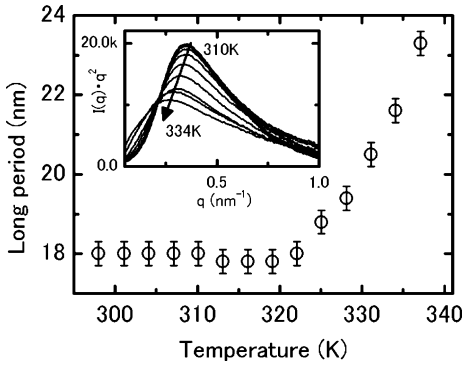

Figure 8. Temperature dependence of the long periods of the PVA film undeformed in water. The inset indicates azimuthally integrated 1-D SAXS profiles, which were used to determine the long periods.

behaviors.[14,19−22] Moreover, this indicates that even at 298 K a large amount of crystallites must dissolve in water compared to the case of the dried film, leading to the difference between the crystallinity of the film in water and that of the dried one at 298 K, as indicated above. Peppas et al. also suggested that the crystallinity of the PVA film decreases immediately in water according to annealing conditions at even room temperature.[23]

In Figure 8, we show the change of the long period of the PVA film in water with increasing temperature. These long periods were determined from the azimuthally integrated 1-D SAXS profiles with the Lorentz correction (typical examples at various temperatures are shown in the inset of Figure 8) of the 2-D scattering patterns by using the Bragg's low. These 2-D scattering patterns were gathered at BL40B2 beamline with the previous described SAXS apparatus.[7] Above the temperature of 338 K, the SAXS peak completely disappears in the 2-D scattering pattern, also indicating that the crystallites fully dissolve below 338 K, as suggested with WAXD results. Below the temperature of 323 K, the long period is kept at constant, although the crystallinity decreases substantially below 323 K, as shown in Figure 7. This indicates that below 323 K crystallites out of the lamellar stacks dissolve with temperature according to the perfection and/or the size of the crystallites because the dissolution of these crystallites does not affect the SAXS intensity in a 2-D SAXS pattern and the long period change but monotonically reduces the crystallinity, as shown in the inset of Figure 7. The dissolution of most of the crystallites in the lamellar stack should occur above 323 K, as shown in Figure 8.

4. Discussion

4.1. Structure Model of the PVA Film Stretched in Water. We previously proposed the preliminary structure model of the PVA film stretched in water, which is schematically shown in Figure 9a, on the basis of the interpretion of the simultaneous stress−strain/SAXS measurement results.[7]

Now, the previously proposed structure changes are reviewed with increasing the strain. Below the strain of 70%, the crystalline lamellae orient to the direction perpendicular to the stretching direction, and the intervening amorphous regions are elastically expanded with the film drawing in proportion to the macroscopic film deformation. Beyond the strain of 70%, the molecular chains in the intermediated amorphous regions are gradually relaxed with the lamellar breakup, which was indicated with the decrease in the longitudinal long period. Above 180% strain, the structural transition of the lamellar structure to the microfibrillar one takes place. Moreover, interfibrillar interaction of the adjacent microfibrils decreases with the film stretching by the pulling out of the tie chains, which are interpenetrating to the adjacent microfibrils, leading to the macroscopic plastic deformation of the PVA film and stress relaxation of most of the microfibrils which is shown by the continuous longitudinal long period decrease.[24−27] In the final stage of deformation, the networking with a long-range connectivity composed of the microfibrils and the interfibrillar extended amorphous chains proceeds associated with the sliding between the adjacent microfibrils with successive drawing. However, the network of the interfibrillar extended amorphous regions is considered to be an origin of the strain-induced hardening,[28,29] which occurs above 180% strain up to a break, because most of the microfibrils are relaxed with strain.

The stress−strain/WAXD results in this study complete the proposed structure model of the PVA film via the decrease in the transversal crystallite size and crystallinity below the strain of 200% and the strain-induced crystallization initiated at the onset of the strain-induced hardening of the film. That is to say, the decrease in the transversal crystallite size and crystallinity below the strain of about 200% confirms the lamellar breakup and the consequent unfolding of molecular chains with strain, as described in our previously proposed model. As mentioned above, the degree of crystalline orientation levels off in the range of 50−200% which also indicates the relaxation of the interlamellar amorphous regions associated with the lamellar breakup above the strain of 50%. In Figure 1, in the stress−strain curve simultaneously obtained, a marked yield drop expected with the relaxation of the molecular chains in the intermediated amorphous regions may not be observed because the amorphous chains swollen with water are fully mobile and the crystallites are easily broken in water, as suggested in section 3.2. This situation is considered to be similar to the case of the segmented elastomers composed of the crystalline blocks (hard segments) and noncrystalline mobile blocks (soft segments) with a low glass transition temperature. In this case, a marked yield drop may not be generally detected in the stress−strain curve. However, at 298 K we can detect a distinct yield point at about 50% strain in the expanded view of the early stage of the stress−strain relationship, as shown in Figure 10, although a marked yield drop cannot be observed.

Furthermore, the occurrence of the strain-induced crystallization above the strain of about 200%, which is identical to the onset strain of the strain-induced hardening, indicates that the strain-induced crystallization takes place in the interfibrillar amorphous regions shown in Figure 9a because only those amorphous regions bear the large stress associated with the

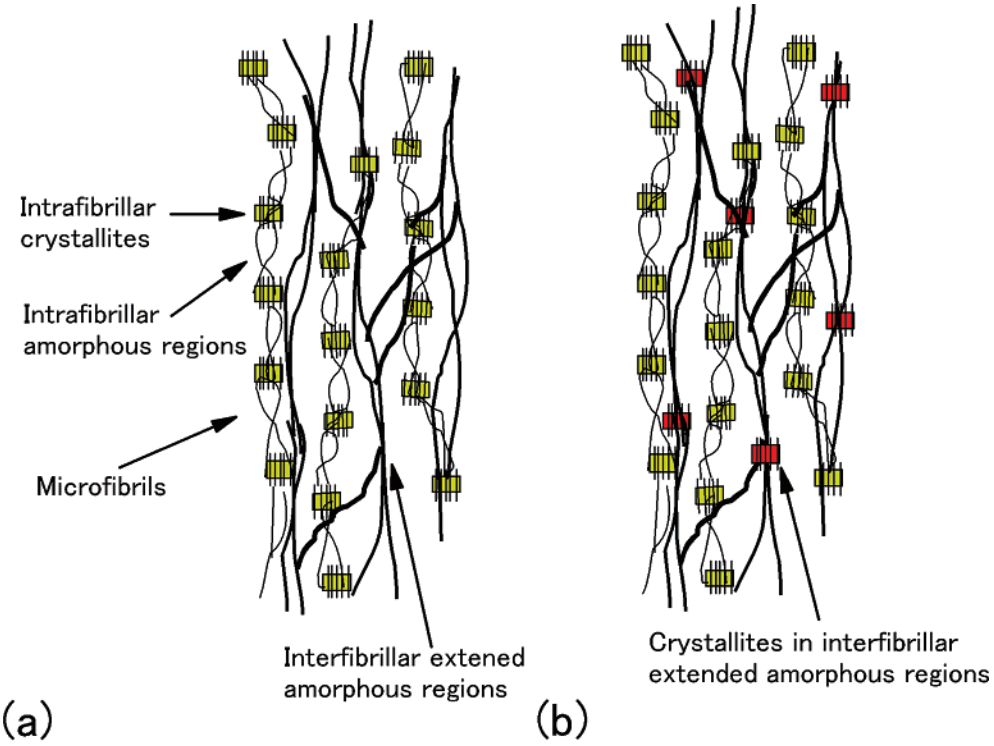

Figure 9. Schematic drawing of the structure model for the PVA film stretched in water: (a) the previous model proposed in the previous paper; (b) the final model proposed in this study. Thick lines: interfibrillar extended amorphous chains; thin lines: intrafibrillar relaxed amorphous chains.

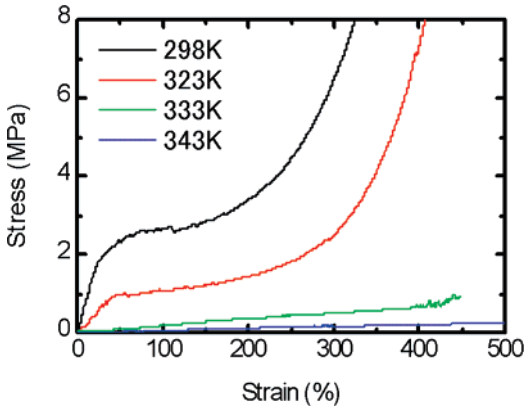

Figure 10. Stress−strain curves for the PVA film in water at various temperatures indicated in this figure using a tensile testing device (AUTO GRAPF) with a homemade water bath.

strain-induced hardening, whereas most of the microfibrils are fully relaxed in this strain range.

Our newly proposed structure model including the strain-induced crystallization in the interfibrillar extended amorphous regions is schematically described in Figure 9b. In our previous paper, it was confirmed that the longitudinal long period decrease is attributed to the microfibrillar relaxation rather than the melting of the crystallites and recrystallization[30−32] or the dislocation in the crystallites[33,34] with strain. Except for these mechanisms, it should be considered that the longitudinal long period decrease may be originated from the strain-induced crystallization in the intrafibrillar amorphous regions in addition to the original crystallites rather than the stress relaxation of the microfibrils with strain. However, the longitudinal long period decrease occurs above the strain of 70%, as described in the previous paper, which is much lower than the onset strain (about 200%) of the strain-induced crystallization and hardening, as described in this study. Therefore, the longitudinal long period decrease should be attributed to the stress relaxation of the microfibrils rather than the strain-induced crystallization in the intrafibrillar amorphous regions. This also confirms that the strain-induced crystallization must take place in the interfibrillar highly extended amorphous regions, which bear the large stress associated with the strain-induced hardening. In turn, the molecular chains in the interfibrillar amorphous regions are fully extended such that the strain-induced crystallization takes place with strain.

4.2. Role of Crystallites on the Stress−Strain Behavior. Figure 10 shows the stress−strain curves of the films at various water temperatures. Below 323 K, the strain-induced hardening takes place prior to a break, whereas above 333 K the film is broken without the stress increase. Above 333 K, the softening of the system should be ascribed to the dissolution of crystallites. The crystallites in the film must play an important role on the strain-induced hardening, although even at 323 K a relatively large amount of crystallites dissolve, as shown in the inset of Figure 7 (half of the crystallinity index at 298 K). In Figure 8, the long period remains constant below 323 K, indicating that the crystallites in the lamellar stacks do not dissolve despite a large decrease in crystallinity below 323 K. In the case of this PVA film, there are many crystallites out of the lamellar stacks which do not affect the long period and the SAXS intensity profile, and these crystallites dissolve at a relatively low temperature compared to those in the lamellar stacks.

In general, it is considered that the lamellar stack acts as a precursor of the microfibril on the film stretching. In this system, the only interfibrillar oriented amorphous regions bear the large stress with strain. Therefore, the strain-induced hardening does not take place without the development of those amorphous regions via the fibrillation of the lamellar stacks with strain. In fact, we performed the stress−strain/SAXS and stress−strain/WAXD simultaneous experiments for the film in water at 333 K, at which crystallites in the lamellar stacks are considered to be dissolving, and found that the SAXS and WAXD intensity profiles associated with the strain-induced crystallization and

fibrillation do not quite appear with strain. This indicates that the interfibrillar extended amorphous regions are not formed in the film at 333 K and that molecular chains in the film are not effectively extended.

It should be noticed that the extended amorphous regions may contribute to the formation of the highly oriented PVA−iodine complexes, when the PVA film is stretched in a KI/I_2 aqueous solution with a relatively low concentration for the preparation of polarizers. Therefore, it must be required that the PVA film is stretched in a KI/I_2 aqueous solution below 323 K for the preparation of a high-performance polarizer.

5. Conclusion

In this article, we present the structure model of a PVA film during uniaxial deformation in water. It contains the strain-induced crystallization in the interfibrillar extended amorphous regions formed with increasing the strain.

Furthermore, it was found that the lamellar stacks in the film contribute to the system hardening, which is attributed to the extension of the interfibrillar amorphous regions, as precursors of the microfibrils formed with increasing the strain. As a result, the system hardening induces the effective molecular chain extension. This may contribute to a high degree of orientation of PVA−iodine complexes, when the PVA film is stretched in a KI/I_2 aqueous solution.

Acknowledgment. The authors thank Dr. S. Sasaki and Dr. K. Masunaga of the Japan Synchrotron Radiation Research Institute (JASRI), Mr. Y. Tsuji and Mr. Y. Yoshida of Kyoto Institute of Technology, and Dr. Y. Sugino of Nitto Denko Corp. for their support on our experiments at SPring-8. The synchrotron radiation experiments were performed at the BL40B2 in the SPring-8 with the approval of JASRI (Proposal No. 2005B0103-NL2b-np, No. 2006A0014-NL2b-np, and No. 2006B1210).

References and Notes

(1) Sakurada, I. *Polyvinyl Alcohol Fibers*; Marcel Dekker: New York, 1985.
(2) Miyasaka, K. *Adv. Polym. Sci.* **1993**, *108*, 91.
(3) Choi, Y. S.; Miyasaka, K. *J. Appl. Polym. Sci.* **1993**, *48*, 313.
(4) Takamiya, H.; Tanahashi, Y.; Matsuyama, T.; Tanigami, T.; Yamaura, K.; Matsuzawa, S. *J. Appl. Polym. Sci.* **1993**, *50*, 1807.
(5) Zwick, M. M. *J. Appl. Polym. Sci.* **1965**, *9*, 2393.
(6) Inagaki, F.; Harada, I.; Shimanouchi, T.; Tasumi, M. *Bull. Chem. Soc. Jpn.* **1972**, *45*, 3384.
(7) Miyazaki, T.; Hoshiko, A.; Akasaka, M.; Shintani, T.; Sakurai, S. *Macromolecules* **2006**, *39*, 2921.
(8) Tashiro, K.; Kobayashi, M.; Tadokoro, H. *Polym. Bull. (Berlin)* **1978**, *1*, 61.
(9) Wu, J.; Schultz, J. M.; Yeh, F.; Hsiao, B. S.; Chu, B. *Macromolecules* **2000**, *33*, 1765.
(10) Wu, J.; Schultz, J. M.; Samon, J. M.; Pangelinan, A. B.; Chuah, H. H. *Polymer* **2001**, *42*, 7131.
(11) Nogales, A.; Sics, I.; Ezquerra, T. A.; Denchev, Z.; Balta, Calleja, F. J.; Hsiao, B. S. *Macromolecules* **2003**, *36*, 4827.
(12) Sakurada, I.; Nukushima, Y.; Mori, N. *Kobunshi Kagaku* **1955**, *12*, 302.
(13) Miyazaki, T.; Katayama, S.; Funai, E.; Tsuji, Y.; Sakurai, S. *Polymer* **2005**, *46*, 7436.
(14) Watase, M.; Nishinari, K. *Makromol. Chem.* **1989**, *190*, 155.
(15) Takigawa, T.; Urayama, K.; Morino, Y.; Masuda, T. *Polym. J.* **1994**, *25*, 929.
(16) Takigawa, T.; Urayama, K.; Masuda, T. *Polym. Gels Networks* **1994**, *2*, 59.
(17) Takigawa, T.; Morino, Y.; Urayama, K.; Masuda, T. *Polym. J.* **1996**, *28*, 1012.
(18) Urayama, K.; Takigawa, T.; Masuda, T. *Macromolecules* **1993**, *26*, 3092.
(19) Watase, M.; Nishinari, K. *J. Polym. Sci., Part B: Polym. Phys.* **1985**, *23*, 1803.
(20) Tanigami, T.; Murase, K.; Yamaura, K.; Matsuzawa, S. *Polymer* **1994**, *35*, 2573.
(21) Peppas, N. A.; Merrill, E. W. *J. Appl. Polym. Sci.* **1976**, *20*, 1457.
(22) Ricciardi, R.; Auriemma, F.; Gaillet, C.; De Rosa, C.; Laupretre, F. *Macromolecules* **2004**, *37*, 9510.
(23) Mallapragada, S. K.; Peppas, N. A. *J. Polym. Sci., Part B: Polym. Phys.* **1996**, *34*, 1339.
(24) Fakirov, S.; Fakirov, C.; Fischer, E. W.; Stamm, M. *Polymer* **1991**, *32*, 1173.
(25) Fakirov, S.; Fakirov, C.; Fischer, E. W.; Stamm, M.; Apostolov, A. A. *Colloid Polym. Sci.* **1993**, *271*, 811.
(26) Fakirov, S.; Denchev, Z.; Apostolov, A. A.; Stamm, M.; Fakirov, C. *Colloid Polym. Sci.* **1994**, *272*, 1363.
(27) Stribeck, N.; Sapoundjieva, D.; Denchev, Z.; Apostolov, A. A.; Zachmann, H. G.; Stamm, M.; Fakirov, S. *Macromolecules* **1997**, *30*, 1329.
(28) Prevorsek, D. C. *J. Polym. Sci., Part B* **1971**, *32*, 343.
(29) Prevorsek, D. C.; Harget, P. J.; Sharma, R. K.; Reimschuessel, A. C. *J. Macromol. Sci., Phys.* **1973**, *B8*, 127.
(30) Peterlin, A. *J. Mater. Sci.* **1971**, *6*, 490.
(31) Meinel, G.; Peterlin, A. *J. Polym. Sci., Polym. Phys.* **1971**, *9*, 1967.
(32) Balta-Calleja, F. J.; Peterlin, A. *J. Macromol. Sci., Phys.* **1970**, *B4*, 519.
(33) Young, R. J.; Bowden, P. B.; Ritchie, J. M.; Rider, J. G. *J. Mater. Sci.* **1973**, *8*, 23.
(34) Brady, J. M.; Thomas, E. L. *J. Mater. Sci.* **1989**, *24*, 3311.

MA070731K